,,

Angle-Resolved Photo-Emission Spectroscopy*

Yiming Teng,† Derap Pena Mukti Sari,‡ and Xingyu Chen§
Université Paris-Saclay
(Dated: June 13, 2025)

We study a Cu(111) single-crystal surface employing ARPES. A tight-binding approximation was used to predict the electronic band structure, focusing on the 4s-band and its associated features. Experimental results obtained using ARPES confirmed theoretical predictions regarding the Fermi surface and band dispersion. The electron effective mass near the band minimum was determined as $m_e^* = 0.469m_e$, in excellent agreement with established literature.

I. INTRODUCTION

Angle-Resolved Photo-Emission Spectroscopy (ARPES) is a powerful experimental technique in condensed matter physics that enables direct probing of the electronic structure of materials. By measuring the kinetic energy and emission angle of photoelectrons ejected from a material's surface under photon illumination, ARPES can map out the energy-momentum relation, known as the electronic band structure, and resolve critical features such as Fermi surfaces. This method provides fundamental insights into the nature of electronic states in crystalline solids.

The principle of ARPES is based on the photoelectric effect: a photon of sufficient energy excites electrons, liberating them from the material. The energy of the emitted electron is related to its initial binding energy, while the emission angle provides momentum information, particularly the two-dimensional in-plane momentum components. As ARPES is surface-sensitive and preserves momentum parallel to the sample's surface, it is especially well-suited for investigating two-dimensional and layered materials, such as graphene, topological insulators, and high-temperature superconductors [1]. Furthermore, it facilitates analysis of quantum well states, charge density waves, and spin-resolved electron properties.

By reconstructing the electronic structure, ARPES serves as an indispensable tool for understanding electronic properties in condensed matter systems. This lab report focuses on employing ARPES to explore Cu(111) sample, analyzing its band structure features to elucidate its electronic properties and underlying physical interactions.

II. THEORETICAL FRAMEWORK

A. Photoemission and ARPES

The photoelectric effect is the fundamental principle of ARPES. Schematically, a high-energy photon with energy $h\nu$ shoots a material and induces the emission of an electron with a kinetic energy E_k. Denote the binding energy of the electron inside the material as E_B, and the work function representing the energy cost of exciting an un-bonded electron at the Fermi level to a free electron at the vacuum level outside the sample as W, then energy conservation implies

$$E_B = h\nu - E_k - W. \tag{1}$$

In an ARPES setup, photons are almost perpendicularly injected to the sample's surface. Consequently, the photoemission electron's wavevector parallel to the surface $\boldsymbol{k}_\parallel$ is conserved. Since the length of the total wavevector of the electron writes

$$|\boldsymbol{k}| = \frac{1}{\hbar}\sqrt{2m_e E_k}, \tag{2}$$

hence, given the polar angle θ and the azimuthal angle φ of $\boldsymbol{k}$, the electron's Bloch wavevector can be reconstructed as

$$\boldsymbol{k}_\parallel = \begin{pmatrix} |\boldsymbol{k}|\sin\theta\cos\varphi \\ |\boldsymbol{k}|\sin\theta\sin\varphi \end{pmatrix}. \tag{3}$$

In this way, the relation between the electron's binding energy E_B and its Bloch wavevector $\boldsymbol{k}_\parallel$ can be established, and the 2-dimensional band structure can be revealed.

B. Cu(111) Surface State: A Tight-Binding Study

The sample in this experiment is Cu(111) single-crystal. Copper usually has a face-centered cubic (fcc) structure, and the Cu(111) single-crystal sample is prepared so that its surface is aligned with the (111) crystal plane. In this way, cooper atoms manifest a hexagonal arrangement on each (111) plane.

* Lab Report at Université Paris-Saclay.
† yiming.teng@universite-paris-saclay.fr
‡ derap-pena-mukti.sari@universite-paris-saclay.fr
§ xingyu.chen@universite-paris-saclay.fr

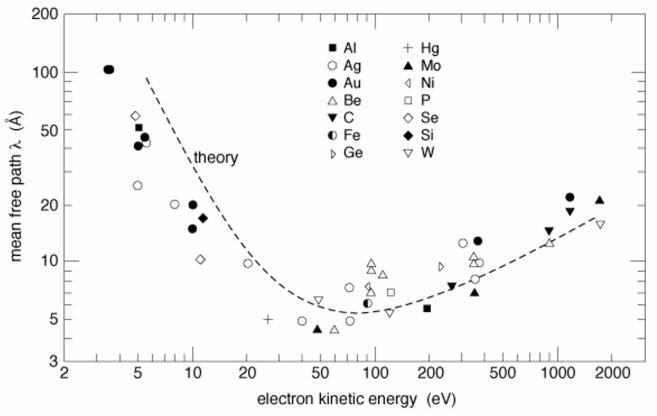

FIG. 1. Mean free path for electrons in various materials.

According to Figure 1, electrons scarcely penetrate materials. Therefore, electrons emitted in a photoemission event are those in the proximity of the surface, and we are assured to regard the actual sample probed in the experiment as a single-layer hexagonal copper lattice, and the direct space structure is illustrated on the left-hand side in Figure 2.

Denote the lattice constant as a, a handy choice of the primitive vectors for the Bravais lattice would be

$$\boldsymbol{a} = a\begin{pmatrix}1\\0\end{pmatrix}, \qquad \boldsymbol{b} = \frac{a}{2}\begin{pmatrix}1\\\sqrt{3}\end{pmatrix}, \tag{4}$$

hence the reciprocal lattice is spanned by the primitive vectors

$$\boldsymbol{a}^* = \frac{2\pi}{a}\begin{pmatrix}1\\-\sqrt{3}/3\end{pmatrix}, \qquad \boldsymbol{b}^* = \frac{4\pi}{\sqrt{3}a}\begin{pmatrix}0\\1\end{pmatrix}. \tag{5}$$

They generate a hexagonal reciprocal lattice, demonstrated on the right-hand side of Figure 2. Here, we also shaded the first Brillouin zone and labeled the high-symmetry points.

The ground state electronic configuration of a single copper atom is $[\mathrm{Ar}]3d^{10}4s^1$. Heuristically, it is the highest $4s$ orbital that contributes to the conduction band intersecting the Fermi surface, and it is this conduction band that we are imaging and are interested in the electron's effective mass near its band edge. In order to fully appreciate the experiment result, we first carry out a theoretical study within the tight-binding framework under the assumption that only the $4s$-orbitals of copper atoms on the hexagonal lattice participate in forming the highest occupied conduction band.

Denote $\{\boldsymbol{R}\}$ as the real-space positions for the copper atoms, and the effective single-electron Hamiltonian is written as $\mathcal{H}$. Suppose the total number of atoms is N, then we can construct a Bloch state $\psi_{\boldsymbol{k}}$ out of single-atom $4s$ wavefucntions ϕ_{4s}:

$$\psi_{\boldsymbol{k}}(\boldsymbol{r}) = \frac{1}{\sqrt{N}}\sum_{\boldsymbol{R}} e^{\mathrm{i}\boldsymbol{k}\cdot\boldsymbol{R}}\phi_{4s}(\boldsymbol{r}-\boldsymbol{R}). \tag{6}$$

Following the spirit of tight-binding approximation, we regard $\psi_{\boldsymbol{k}}(\boldsymbol{r})$ as a good approximation of the eigenstate for the Hamiltonian $\mathcal{H}$, hence the energy band writes

$$\begin{aligned}
E_{4s}(\boldsymbol{k}) &= \langle\psi_{\boldsymbol{k}}|\mathcal{H}|\psi_{\boldsymbol{k}}\rangle \\
&= \frac{1}{N}\sum_{\boldsymbol{R},\boldsymbol{R}'} e^{\mathrm{i}\boldsymbol{k}(\boldsymbol{R}-\boldsymbol{R}')}\int \mathrm{d}\boldsymbol{r}\ \phi_{4s}^*(\boldsymbol{r}-\boldsymbol{R}')\mathcal{H}\phi_{4s}(\boldsymbol{r}-\boldsymbol{R}) \\
&= \frac{1}{N}\sum_{\boldsymbol{R},\boldsymbol{R}'} e^{\mathrm{i}\boldsymbol{k}(\boldsymbol{R}-\boldsymbol{R}')}\int \mathrm{d}\boldsymbol{r}\ \phi_{4s}^*(\boldsymbol{r})\mathcal{H}\phi_{4s}(\boldsymbol{r}-(\boldsymbol{R}-\boldsymbol{R}')) \\
&= \sum_{\boldsymbol{R}} e^{\mathrm{i}\boldsymbol{k}\cdot\boldsymbol{R}}\int \mathrm{d}\boldsymbol{r}\ \phi_{4s}^*(\boldsymbol{r})\mathcal{H}\phi_{4s}(\boldsymbol{r}-\boldsymbol{R}).
\end{aligned} \tag{7}$$

Let's assume only homogeneous nearest-neighbor transitions and denote[2]

$$\varepsilon_0 \equiv \int \mathrm{d}\boldsymbol{r}\ \phi_{4s}^*(\boldsymbol{r})\mathcal{H}\phi_{4s}(\boldsymbol{r}), \tag{8}$$

$$t \equiv \int \mathrm{d}\boldsymbol{r}\ \phi_{4s}^*(\boldsymbol{r})\mathcal{H}\phi_{4s}(\boldsymbol{r}-\boldsymbol{\tau}) < 0, \tag{9}$$

where $\boldsymbol{\tau}$ is an arbitrary vector connecting a nearest neighbor. In this way, the energy band writes

$$E_{4s}(\boldsymbol{k}) = \varepsilon_0 + t\sum_{\boldsymbol{\tau}} e^{\mathrm{i}\boldsymbol{k}\cdot\boldsymbol{\tau}}. \tag{10}$$

For our hexagonal case, the summation over $\boldsymbol{\tau}$ goes through $\{\boldsymbol{a},\boldsymbol{b},-\boldsymbol{a},-\boldsymbol{b},\boldsymbol{b}-\boldsymbol{a},\boldsymbol{a}-\boldsymbol{b}\}$, and the band turns to be

$$E_{4s}(\boldsymbol{k}) = \varepsilon_0 + 2t\left(\cos k_x + 2\cos\frac{k_x}{2}\cos\frac{3k_y}{2}\right). \tag{11}$$

This band is visualized in Figure 3 over an extended region in the reciprocal space and in Figure 4 near the first Brillouin zone. Within the first Brillouin zone, the band takes the minimum at the Γ-point while is maximal at the K, K'-points. The M-point behaves like a saddle point in the extended zone scheme.

III. EXPERIMENTAL APPARATUS

As illustrated in Figure 6, the instrumentation of ARPES contains two major parts:

- Light source: The monochromaticity of the light source is crucial to measuring electronic structures accurately. In this experiment carried out at the TEMPO beamline at Soleil, the monochromatic light is provided by the synchrotron radiation filtered by a monochromator. Designed to be a soft X-ray beamline, the energy of the light source ranges from 50 eV to 1500 eV, offering us the possibility to study both the high-lying and deeper energy bands.

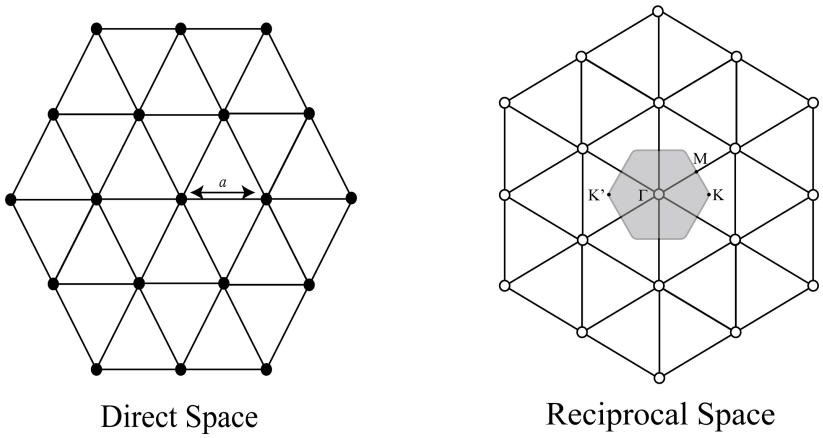

FIG. 2. Direct space and reciprocal space structures of the surface of the Cu(111) sample. High-symmetry points in the shaded first Brillouin zone are highlighted.

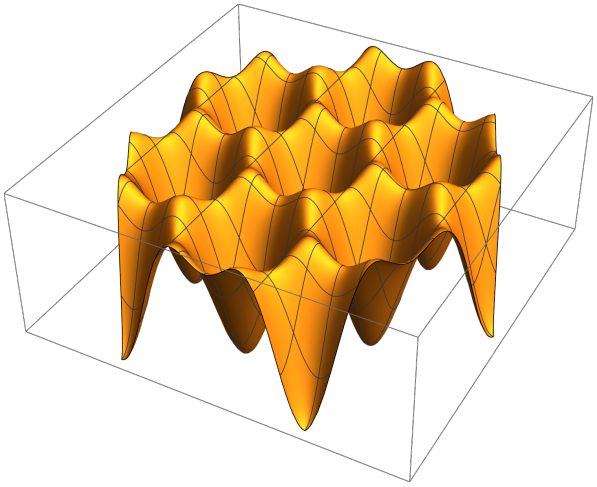

FIG. 3. Overview on the 4s band.

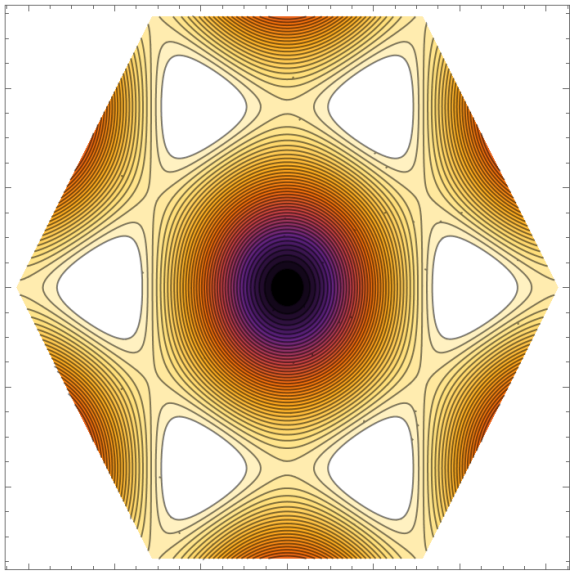

FIG. 4. Contour plot of the 4s band near the first Brillouin zone.

- Photoelectron analyzer: The determination of the photoelectrons' angles and energies are realized in the hemispherical analyzer. By fixing the azimuthal angle φ and measuring the photoelectron's energies for different polar angles θ, the relation between the band energy $E(\boldsymbol{k}_{\parallel})$ and the length of $\boldsymbol{k}_{\parallel}$ can be established. By varying θ and φ at the same time, the occupied bands can be directly imaged.

IV. DATA ANALYSIS

A. Data Presentation

We first probed the sample's Fermi surface structure (Figure 5) and the dispersion relation of the 4s band near the Γ-point (Figure 7).

The shape of the Fermi surface shown in Figure 5 wonderfully matches our theoretical prediction of the 4s-band with tight-binding approximation. Comparing Figure 5 with Figure 4, we can deduce that the center of Figure 5 (a) surrounded by a circle corresponds to the Γ-point; the bright X-patterns in Figure 5 (b) and Figure 5 (c) are located at the M-points; and the center of the vacant triangle in Figure 5 (c) is the K-point. As for the dispersion relation near the Γ-point shown in Figure 7, we point out that there is an error in labeling the vertical axis that it shouldn't be labeled with angle "deg" but should be labeled with the photoelectron's energy in electrovolts.

We also measured the density of states for the low-lying bands with two different photon energies, and the result is shown in Figure 8. The signal intensity for 1300 eV photon energy is weaker than that for 1200 eV because

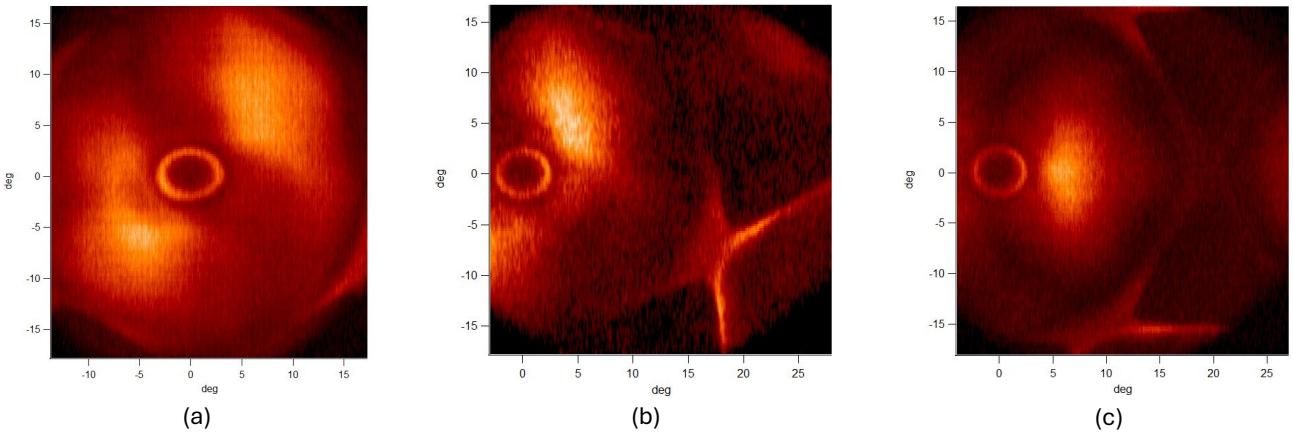

FIG. 5. Fermi surface structure of Cu(111) sample. Different regions of the reciprocal space are accessed by varying the scanning range of the spherical angles (θ, φ).

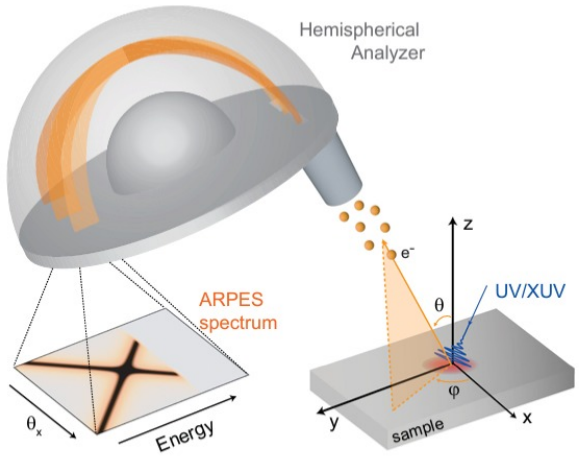

FIG. 6. Schematic illustration of the ARPES experiments apparatus[3].

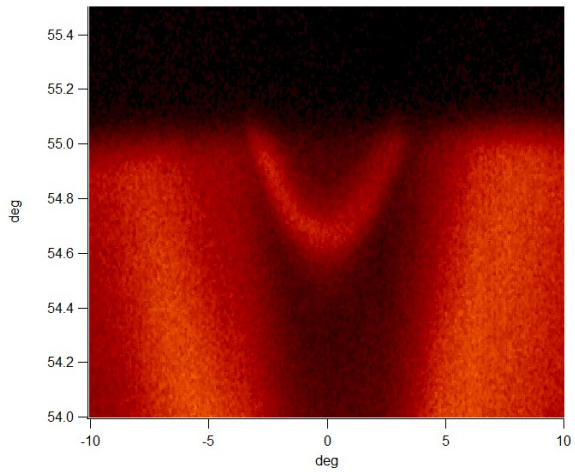

FIG. 7. Dispersion relation near the Γ-point.

the synchrotron produces a smaller 1300 eV photon flux compared to 1200 eV. As the photon's energy increases by 100 eV, all peaks corresponding band electrons are shifted to the right by approximately 100 eV. In particular, for the two prominent peaks corresponding to the bands originating from copper's $2p$ orbital, we find their position shifts are

$$247.524\ \text{eV} \ \rightarrow\ 348.524\ \text{eV}, \quad 267.533\ \text{eV} \ \rightarrow\ 368.034\ \text{eV}.$$

Both of them are approximately shifted by 101 eV, where the 1 eV deviation from the expected value 100 eV is supposed to come from a systematic error on the determination of photon energy at the monochromator. Moreover, given the work function on Copper's (111) face is $W = 4.94$ eV [4], the binding energy for these two bands are determined to be

$$E_{2p,1} = 947.54\ \text{eV}, \quad E_{2p,2} = 927.53\ \text{eV}.$$

It's also worth noting that there are three very weak peaks located within the energy interval 750 eV $\sim$ 930 eV which doesn't move as we increase the photon energy; they correspond to the Auger electron emission: As the injecting photon removes a core electron and creating a vacancy, an electron from a higher energy level may fall into this vacancy and release energy. The released energy can be transferred to a valence electron and ejected out of the atom, resulting in the Auger electron emission. Therefore, the energies of the Auger electron peaks only depend on the atomic properties of the sample and are independent of the photon energy as long as it's high enough to excite core electrons. We remark that, in principle, it should be possible to determine the transitions corresponding to these Auger peaks, but it's beyond the scope of our current report.

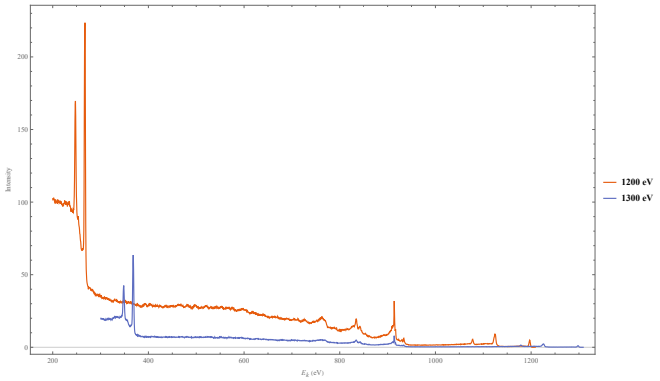

FIG. 8. Measured density of states for low-lying bands.

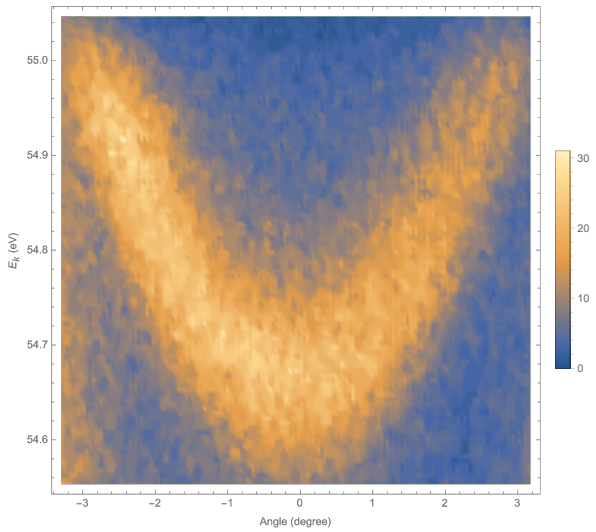

FIG. 9. Plot of the measured 4s-band near the Γ-point.

B. Effective Mass Determination

We now introduce our fully digitized determination of the effective electron mass for the 4s-band near the Γ-point based on the measurement of dispersion in Figure 7.

We first read the data provided in the file `surface_state.txt`, assigning each matrix element its corresponding angle and kinetic energy E_k according to Figure 7. The selected parabolic dispersion curve we are interested in is plotted in Figure 9.

Now, we have to rescale the horizontal axis so that it corresponds to the length of the 2D planar momentum $\boldsymbol{k}_{\parallel}$ based on Equation 2 and Equation 3. We would like to point out that there's no need to convert the vertical scale to the binding energy since it only serves as a global shift in the energy, and it has no influence on the band's curvature, hence not related to the determination of effective mass. The rescaling doesn't distort the plotted band shape and remains resembling Figure 9.

The next step is the removal of background noise. We expect to preserve all the data in the neighborhood of the parabola but filter the rest of the data. Based on the observation that points near the parabola have a significantly larger value compared to other regions, we adopt a straightforward method in which we set a threshold $\vartheta = 18$. Data-point values exceeding ϑ are preserved, while those below it are set to zero. Data after this filtering is plotted in Figure 10.

To determine the center of the parabola, we sample 400 points along the horizontal axis in Figure 10 and calculated the average of the vertical coordinate weighted by the data point's value as the center of the parabola curve. The generated data points and the fitted parabolic curve are shown in Figure 11. In particular, the fitted dispersion relation reads

$$E = 0.08132k^2 + 0.00097k + 54.6738 \text{ (eV)}, \tag{12}$$

where the dimension of k is nm^{-1}. Converting to the international unit, we find the electron's effective mass is

$$m_e^* = 4.27362 \times 10^{-31} \text{ kg} = 0.469 m_e. \tag{13}$$

This result excellently matches the expected reference value $m_e^* = 0.46 m_e$.

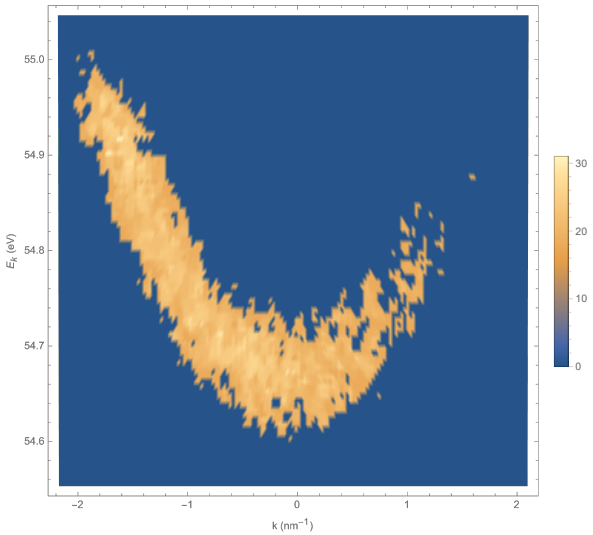

FIG. 10. Filtered data only preserving the major part of the 4s-band parabola.

V. CONCLUSION

We utilized ARPES to investigate the electronic properties of a Cu(111) single-crystal surface. The theoretical analysis, underpinned by the tight-binding approximation, provided a foundational understanding of the 4s-band structure of our sample surface. Experimental data confirmed key theoretical predictions, including the shape of the Fermi surface and the dispersion relation near high-symmetry points, demonstrating excellent alignment between the calculated and measured results.

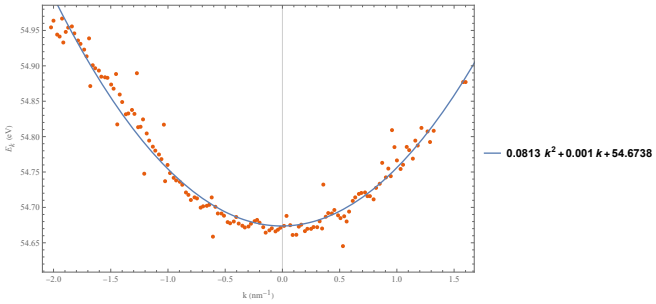

FIG. 11. Generated data points for the parabolic dispersion relation and the fitted curve.

Moreover, the study determined the effective mass of the electrons near the band minimum, yielding a value of $m_e^* = 0.469 m_e$, consistent with established literature.

In conclusion, the experiment underscores the power of ARPES as a tool for mapping electronic structures with high precision. The insights gained about the Cu(111) surface not only validate theoretical models but also enrich our understanding of electronic properties in crystalline materials.

Appendix A: Data Availability

All the raw data and the source code for the data analysis can be accessed through the repository `https://github.com/Yiming-Teng/LEED_ARPES_Analysis.git`.

[1] Wikipedia contributors. Angle-resolved photoemission spectroscopy — Wikipedia, the free encyclopedia. `https://en.wikipedia.org/w/index.php?title=Angle-resolved_photoemission_spectroscopy&oldid=1234808661`, 2024. [Online; accessed 17-December-2024].

[2] Here $t < 0$ is actually an *ad hoc* assumption to reproduce the desired band shape.

[3] Hongyun Zhang, Tommaso Pincelli, Chris Jozwiak, Takeshi Kondo, Ralph Ernstorfer, Takafumi Sato, and Shuyun Zhou. Angle-resolved photoemission spectroscopy. *Nature Reviews Methods Primers*, 2(1):1–22, July 2022.

[4] P. O. Gartland, S. Berge, and B. J. Slagsvold. Photoelectric work function of a copper single crystal for the (100), (110), (111), and (112) faces. *Phys. Rev. Lett.*, 28:738–739, Mar 1972.